

# DensityX: A program for calculating the densities of magmatic liquids up to 1,627 °C and 30 kbar

Kayla Iacovino\* $^{\alpha}$ , Christy B. Till $^{\alpha}$ 

<sup>α</sup>School of Earth and Space Exploration, Arizona State University, Tempe, AZ 85287-6004, USA.

## **ABSTRACT**

Here we present a standalone program, DensityX, to calculate the densities of dry and hydrous silicate melts given pressures, temperatures, and major oxide compositions in wt% in the 10-component system  $SiO_2-TiO_2-Al_2O_3-Fe_2O_3-FeO-MgO-CaO-Na_2O-K_2O-H_2O$ . Here we use DensityX to analyze over 3,000 melt inclusions over a wide compositional range to visualize the distribution of natural silicate liquid densities in the Earth's crust. The program is open-source, written in Python (as a library hosted in PyPi or as a downloadable Python script), and can be accessed and run via an online interface through a web browser at https://densityx.herokuapp.com or by downloading and running the code from a github repository. A companion Excel spreadsheet can also be used to run density calculations identical to those in the Python script but only for one sample at a time. In another example application, we demonstrate how DensityX can be used to constrain density-driven convective cycling in the phonolitic lava lake of Erebus volcano, Antarctica.

Keywords: Magma storage; Magma density; Computational tools; Python; Open source; Silicate liquid; Igneous petrology

#### 1 Introduction

The density of a silicate melt affects a myriad of physical and magmatic processes, including magma mixing [Grove and Baker 1983; Jull and Kelemen 2001], melt migration dynamics [Stolper et al. 1981; Hack and Thompson 2011], and crustal storage [Sparks and Huppert 1984; Walker 1989; Chaussard and Amelung 2014]. Together, these processes lead to the diversity of magma types observed on Earth. Melt density is also an important parameter in planetary differentiation, where density-driven stratification segregates a planetary body into a crust, mantle, and core [Agee and Walker 1988; Ohtani 1985; Circone and Agee 1996]. A significant amount of effort has been put into modeling silicate melt densities, which relies upon determination of thermodynamic parameters such as partial molar volumes of major oxide from experiments conducted at a range of pressure (P) and temperature (T) conditions and expressions describing changes in the volume of these components as a function of P and T (e.g., related to thermal expansion and compressibility of ions). Much of this work was pioneered by R.A. Lange, V.C. Kress, and coworkers who produced a series of papers describing the densities of the major components of silicate liquids [Lange and Carmichael 1987], thermodynamic relations needed to calculate silicate melt density at elevated P and T [Lange and Carmichael 1990; Kress

and Carmichael 1991; Lange 1997], and the important addition of thermodynamic data related to the density of H<sub>2</sub>O in silicate melts [Ochs III and Lange 1999; Richet et al. 2000]. This work resulted in an equation of state (EOS) for silicate melts in the 10-component system SiO<sub>2</sub>-TiO<sub>2</sub>-Al<sub>2</sub>O<sub>3</sub>-Fe<sub>2</sub>O<sub>3</sub>-FeO-MgO-CaO-Na<sub>2</sub>O-K<sub>2</sub>O-H<sub>2</sub>O [Lange and Carmichael 1990]. The thermodynamic values underpinning these models (e.g. liquid partial molar volumes and melt compressibilities) were recalibrated by Ghiorso [2004], who increased the size of the database used for earlier calibrations and provided a more rigorous treatment of the effect of the oxidation state of Fe on the densities of melts. In the Ghiorso-Kress approach, Fe-bearing systems are speciated into three (rather than two) components: FeO, Fe<sub>2</sub>O<sub>3</sub>, and FeO<sub>1.3</sub>. This new treatment and expanded database resulted in an improved model recovery of density measurements in Fe-bearing systems but requires knowledge of the melt oxygen fugacity.

Over the last four decades, research in this area has produced a large knowledge base of thermodynamic relations as well as the formulae needed to interpret geologic data. The resulting formulae for density calculations are typically presented as thermodynamic equations in the literature or integrated into larger thermodynamic modeling programs such as MELTS (first published as Ghiorso and Sack [1995]), Perple\_X [Connolly 2005], Theriak\_D [Duesterhoeft and de Capitani 2013], and the model of Fluegel [2007], which rely on the above mentioned published datasets. However,

<sup>\*</sup>Corresponding author: kayla.iacovino@nasa.gov Now at: Jacobs, NASA Johnson Space Center, 2101 NASA Pkwy, Houston, TX 77058, USA.

no standalone program for calculating the density of a silicate melt as a function of *P* and *T* exists, making the calculation cumbersome. Automated calculations within currently available thermodynamic modeling programs are useful but require a working knowledge of each program's infrastructure, are time consuming to perform on very large datasets, and the inclusion of the density calculation within the programs means that it is not readily extensible by the end-user.

Here we present a standalone program, called DensityX, to calculate the densities of hydrous silicate melts given pressures, temperatures, and major oxide compositions in wt% in the 10-component system  $SiO_2-TiO_2-Al_2O_3-Fe_2O_3-FeO-MgO-CaO-Na_2O-K_2O-H_2O$ , using thermodynamic data for these components from Lange and Carmichael [1987], Lange [1997], Kress and Carmichael [1991], and Ochs III and Lange [1999].

## 2 Program DensityX

The program DensityX is based on previously published thermodynamic properties of silicate liquids given in Lange and Carmichael [1987], Lange and Carmichael [1990], and Ochs III and Lange [1999] and equations to describe the pressure- and temperaturedependent partial molar volumes of oxide components given in Lange and Carmichael [1990]. The density of a silicate melt depends upon the individual densities of the oxide components of the melt, which in turn depend on their partial molar volumes. Partial molar volumes of the components will depend upon several factors, including overall melt composition, degree of melt polymerization, and changes to coordination of cations with pressure. Here we use an empirical description of melt density, which assumes ideal mixing between components [Lange and Carmichael 1990]:

$$\rho_{liq} = \frac{\sum [X_i M_i]}{V_{liq}} \tag{1}$$

where  $\rho_{liq}$  is the density of the silicate liquid,  $X_i$  is the mole fraction and  $M_i$  is the molecular weight of oxide component i in the melt, and  $V_{liq}$  is the volume of the silicate liquid at a given P and T defined as the sum of the partial molar volumes of each oxide component at P and T and normalized to the concentration of each component, as:

$$V_{liq} = \sum X_i \overline{V}_i \tag{2}$$

where  $\overline{V}_i$  is the calculated partial molar volume at given P and T of the oxide component i in the melt.

To calculate melt density at P and T, DensityX first calculates the individual molar volumes of each component oxide at P and T. We use a simplified model equation that incorporates the effects of pressure  $(d\overline{V}_i/dP)$ 

and temperature  $(d\overline{V}_i/dT)$  on volume, which is sufficient to describe the volume of natural liquids up to 30 kbar [Lange and Carmichael 1990]:

$$V_{liq}(X_i, T, P) = \sum_{i} \left[ \overline{V}_i(T_{ref}, 1 \text{ bar}) + \frac{d\overline{V}_i}{dT} + \frac{d\overline{V}_i}{dP} (P - 1 \text{ bar}) \right] X_i \quad (3)$$

where  $V_i(T_{ref},1)$  bar) is the partial molar volume of component i in the liquid at reference temperature  $T_{ref}$  and a pressure of 1 bar and  $d\overline{V}_i/dT$  and  $d\overline{V}_i/dP$  are the temperature and pressure derivatives of the partial molar volume of component i. The pressure dependence of the partial molar volume will be stronger with pressure, and so the second pressure derivative  $d^2V_i/dP^2$  would be required to calculate  $V_i$  at P > 30 kbar [Lange and Carmichael 1990].

DensityX employs the EOS of Lange and Carmichael [1990], since the updated Ghiorso-Kress EOS requires knowledge of the system's oxygen fugacity, which is often not known (or not reported) for both natural and experimental samples. A comparison of density values calculated with the DensityX and Ghiorso-Kress databases are given in Appendix 1. Values used in the DensityX model are calibrated for silicate melt compositions ranging from:  $SiO_2 = 37-75$  mol%;  $TiO_2 \le 4$ mol%;  $Al_2O_3 \le 27$  mol%;  $Fe_2O_3 \le 15$  mol%;  $MgO \le 15$ 38 mol%; CaO  $\leq$  43 mol%; Na<sub>2</sub>O  $\leq$  33 mol%; K<sub>2</sub>O  $\leq$ 29 mol%; and H<sub>2</sub>O < 19 mol% [Lange 1997; Ochs III and Lange 1999]. The model is valid in the range 1-30 kbar [Lange and Carmichael 1990] and from the glass transition temperature for any given melt up to 1627 °C (1900 K; [Lange 1997]). Below the glass transition temperature, rearrangements in the glass structure become kinetically impeded, and so a correction must be applied when calculating the density of a glass below this temperature. This requires knowledge of the compositionally dependent values for the glass transition temperature and coefficient of thermal expansion, and so this correction is not applied in DensityX. Calculations at temperatures below the glass transition will therefore have higher error than reported here.

## 3 Description of the program package

DensityX is capable of performing batch calculations on large sample sets (thousands of discrete samples) automatically. The calculation of each sample density is performed iteratively (not in parallel), but the execution is fast. The example input file used here (and available with the model code and online interface) contains over 3,000 individual samples and was processed in <10s during testing (3 GHz Intel Core i7 processor). The code is open source and simple enough to allow the end-user to adjust or update the program with minimal working knowledge of the computer language Python. DensityX is also packaged

	$\overline{V}_i \pm 1\sigma$ (cm <sup>3</sup> /mol)	$d\overline{V}_i/dT \pm 1\sigma$ $(10^{-3} \text{ cm}^3/\text{mol-K})$	$\frac{d\overline{V}_i/dP \pm 1\sigma}{(10^{-4} \text{ cm}^3/\text{mol-bar})}$
SiO <sub>2</sub> TiO <sub>2</sub> Al <sub>2</sub> O <sub>3</sub> Fe <sub>2</sub> O <sub>3</sub>	$26.86 \pm .03$ $28.32$ $37.42 \pm .09$ $41.5$	- 7.24 2.62 0	$-1.89 \pm .02$ $-2.31 \pm .06$ $-2.26 \pm .09$ $-2.53 \pm .09$
FeO MgO CaO Na <sub>2</sub> O	$12.68$ $12.02 \pm .07$ $16.9 \pm .06$ $29.65 \pm .07$	3.69 3.27 3.74 7.68	$-0.45 \pm .03$ $0.27 \pm .07$ $0.34 \pm .05$ $-2.40 \pm .05$
$K_2O$ $H_2O$	$47.28 \pm .10$ $22.9 \pm .60$	$12.08$ $9.5 \pm .8$	$-6.75 \pm .14$ $-3.20 \pm .60$

Table 1 – Partial molar volumes and pressure and temperature derivatives for each oxide component.

Partial molar volumes for: SiO<sub>2</sub>, Al<sub>2</sub>O<sub>3</sub>, MgO, CaO, Na<sub>2</sub>O, K<sub>2</sub>O at  $T_{ref}$  =1773 K [Lange 1997]; TiO<sub>2</sub>, at  $T_{ref}$  =1773 K [Lange and Carmichael 1987]; Fe<sub>2</sub>O<sub>3</sub> at  $T_{ref}$  =1723 K [Liu 2006]; FeO at  $T_{ref}$  =1723 K [Guo et al. 2014]; H<sub>2</sub>O at  $T_{ref}$  =1273 K [Ochs III and Lange 1999].  $d\overline{V}_i/dT$  values for: SiO<sub>2</sub>, TiO<sub>2</sub>, Al<sub>2</sub>O<sub>3</sub> from [Lange and Carmichael 1987]; MgO, CaO, Na<sub>2</sub>O, K<sub>2</sub>O from Lange [1997]; Fe<sub>2</sub>O<sub>3</sub> from Liu [2006]; FeO from Guo et al. [2014]; H<sub>2</sub>O from Ochs III and Lange [1999].  $d\overline{V}_i/dP$  values for anhydrous components from Kress and Carmichael [1991]: H<sub>2</sub>O from Ochs III and Lange [1999].

as a Python library, called densityx, hosted with PyPi and can be installed using pip. A supplementary version of the code is given as a Microsoft Excel spreadsheet (Supplementary file 1), which performs the same calculations as the Python program but can only calculate the density of one sample at a time. The program can be accessed and run completely within a browser at https://densityx.herokuapp.com or can be downloaded and run locally from https://github.com/kaylai/DensityX.

Instructions on installation and implementation of the DensityX.py script and densityx library are available on the github repository.

For batch calculations, an input file with the oxide compositions, P, and T of each sample must be prepared by the user. The file test-data.xlsx is included with the program (and can be downloaded via the web interface) and serves as a template for an input file. Although this file can have any name, it must follow the structure of test-data.xlsx, with columns named as follows (with composition in wt%, pressure in bars, and T in °C): Sample\_ID, SiO<sub>2</sub>, TiO<sub>2</sub>, Al<sub>2</sub>O<sub>3</sub>, Fe<sub>2</sub>O<sub>3</sub>, FeO, MgO, CaO, K<sub>2</sub>O, H<sub>2</sub>O, P, T. The order of the columns does not matter, as the program locates data columns in the input file based on the column name given in the first row of the file. If using the densityx Python library, a Pandas DataFrame with the column names as described above serves as input data. On the web interface, or if using the DensityX.py script, the user will be prompted to browse for a .xlsx file.

Upon choosing the input file (or upon passing a Pandas DataFrame), the following operations are done on the data to calculate density. First, necessary constants

are defined for all oxide components (Table 1): molecular weights; partial molar volumes at the reference P and T of 1 bar and 1773 K,  $\overline{V}_i$  [Lange and Carmichael 1987; Lange 1997; Ochs III and Lange 1999]; thermal expansion coefficients expressed as the temperature derivative of  $\overline{V}_i$ ,  $d\overline{V}_i/dT$  [op. cit.]; and compressibility coefficients expressed as the pressure derivative of  $\overline{V}_i$ ,  $d\overline{V}_i/dP$  [Kress and Carmichael 1991; Ochs III and Lange 1999].

The program then solves Equation 1 for each sample in the input file in two steps: by solving first for the numerator (Equation 2) and then for the denominator (the liquid volume, Equation 3). The data is then written to an excel spreadsheet and saved as [Input File Name]\_output.xlsx to the folder where the input file exists. When using the densityx library, a Pandas DataFrame containing density values is returned (see /1ib/README.md available in the github repository for more information on how to interact with the densityx library).

### 4 Densities of natural silicate liquids

As magma bodies ascend, cool, crystalize, and degas, the density of the liquid component will change due to a number of processes including: decreasing pressure during crustal ascent; decreasing temperature during magma storage and cooling; increasing temperature due to magma mixing or mafic recharge events; changing major element composition during differentiation; and changing H<sub>2</sub>O concentration during magma ascent and/or volatile exsolution.

To illustrate the compositional dependence of the

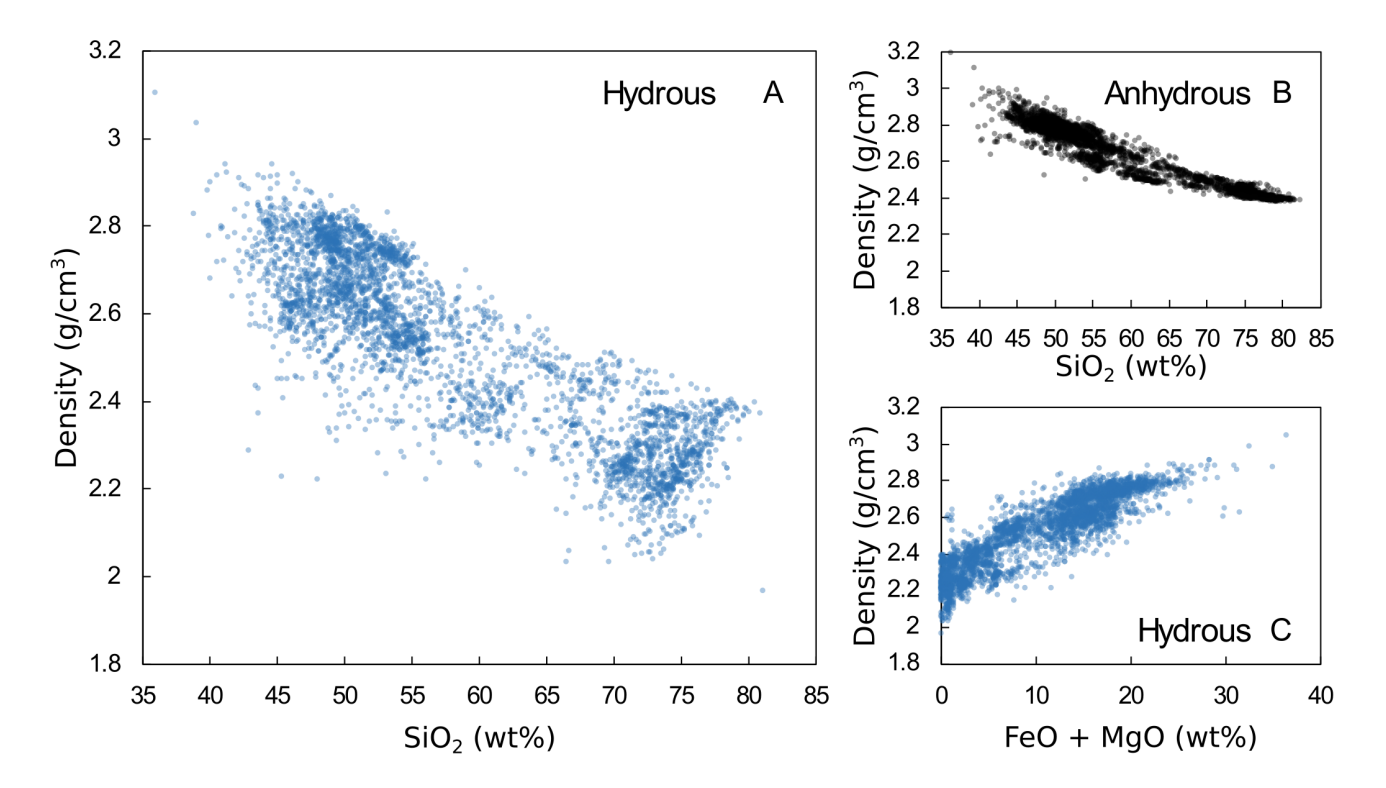


Figure 1: Calculated densities of over 3,000 melt inclusions (normalized to 100%) from volcanic settings around the world. All data from the GEOROC database (http://georoc.mpch-mainz.gwdg.de/georoc/). [A] The spread of densities of different magma types classified based on SiO<sub>2</sub> concentration, including reported H<sub>2</sub>O concentrations. [B] The spread of densities calculated for anhydrous natural magmas. [C] MgO plus total Fe expressed as FeO shows a strong correlation with density, shown here for calculations including reported H<sub>2</sub>O concentrations.

density of natural silicate liquids, geochemical data for over 3,000 crystal-hosted melt inclusions from volcanic settings around the world ranging in SiO<sub>2</sub> concentration from ~40-80 wt% were compiled from the GEOROC database (Figure 1; data from GEOROC http://georoc.mpch-mainz.gwdg.de/georoc/). melt inclusions represent residual liquids isolated from crystallizing magma bodies in the Earth's crust. Because the *P* and *T* of melt inclusion entrapment is rarely known or reported, all samples were run at P = 5,000bar and T = 1,100 °C, representing magma storage conditions in the mid-crust. DensityX was used to calculate the densities of all samples in this dataset in two model runs: one using anhydrous compositions and one including reported dissolved H<sub>2</sub>O concentrations. The data used here are given test-data.xlsx (Supplementary file 2).

Anhydrous melt inclusion compositions range in density from ca. 2.4–3.0 g/cm<sup>3</sup> (Figure 1B). Of the anhydrous components,  $SiO_2$  and mafic components  $MgO+FeO^*$  correlate most strongly with melt density ( $R^2=0.91$ , 0.81 respectively). This is likely due in part to the relative abundance of these oxides in silicate melts and to the propensity of  $SiO_2$  concentration to be anticorrelative with MgO+FeO in natural silicate melts. When reported  $H_2O$  concentrations are included in the

model run, the density range increases significantly to ca. 2.0–3.0 g/cm<sup>3</sup>, with a much higher variability in density for any given magma composition (Figure 1A).  $\rm H_2O$  exhibits such a strong control on density due to its molecular abundance in natural liquids ( $\rm H_2O$  commonly accounts for up to ~25 mol% in silicate melts) and its large partial molar volume ( $\rm \overline{V}_{H_2O} = 22.9 \pm 0.6$  cm<sup>3</sup>/mol; [Ochs III and Lange 1999]) relative to other major oxide components.

During magma ascent and differentiation, pressure and temperature changes will play a strong role on the evolution of the liquid melt density. DensityX was run for a mid-ocean ridge basalt [Dixon et al. 1995] and a high-silica rhyolite [Wallace et al. 1999] with varying  $\rm H_2O$  concentrations from ca. 0–10% over a range of T at P=5,000 bar and over a range of P at T=1,000 °C (Figure 2).

The dependence of liquid density on temperature increases with increasing  $\rm H_2O$  concentration and/or decreasing  $\rm SiO_2$  concentration. Thus, T has the strongest effect on hydrous basalts and the smallest effect on dry rhyolitic melts. In basalt, an addition of 1 wt%  $\rm H_2O$  has an effect on liquid density equivalent to an increase in T of ~300 °C or a decrease in P of ~4,000 bar. In rhyolite, that effect is equivalent to an increase in T of ~500 °C or a decrease in P of ~2,500 bar. This effect is particularly important when calculating densi-

<sup>\*</sup>total Fe as FeO

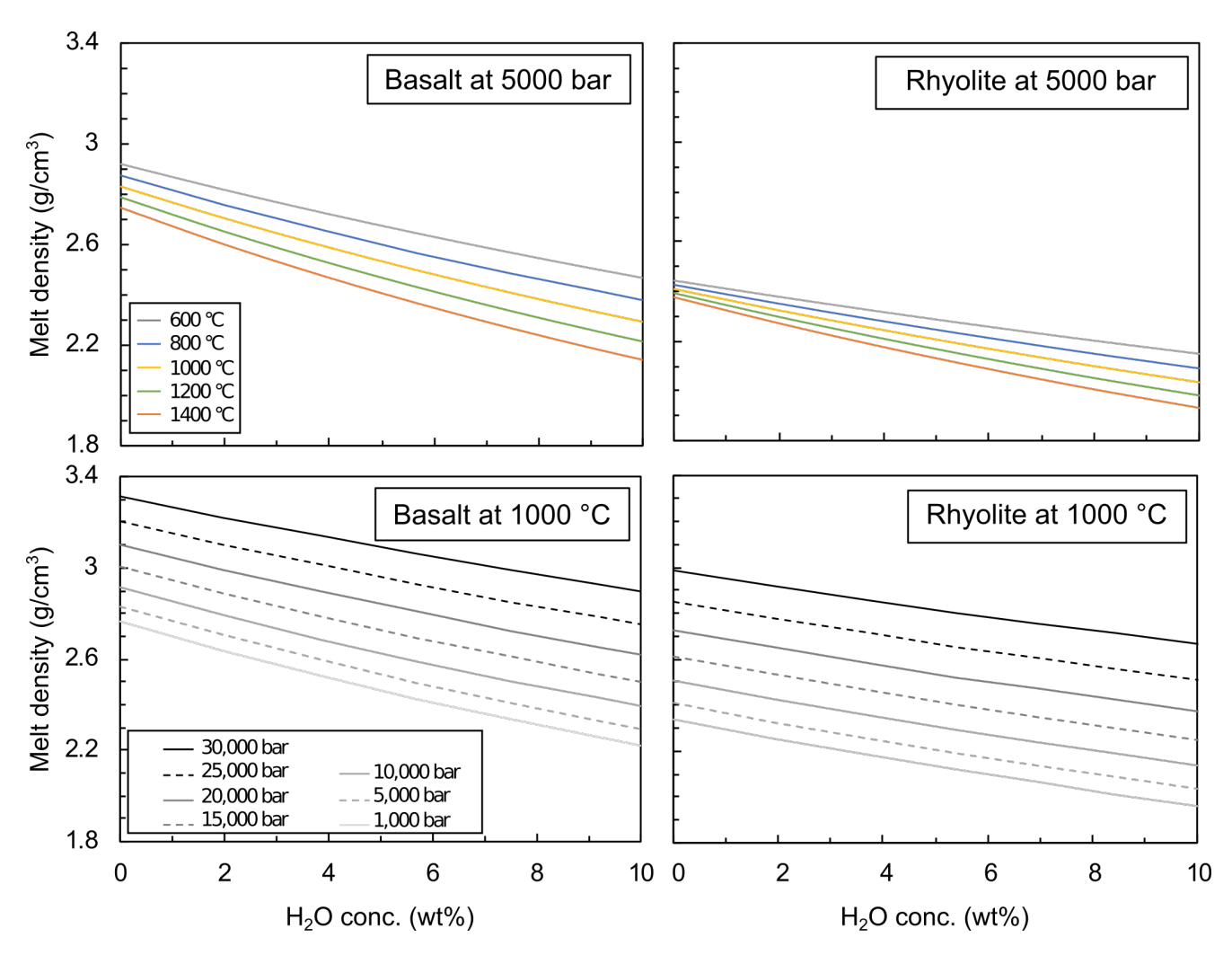


Figure 2: The effect of pressure and temperature on the density of basaltic and rhyolitic melt. Anhydrous basalt composition: sample TT152-21-35 as reported in Dixon et al. [1995] using an  $Fe_2O_3/FeO$  ratio from experiment #7 (op cit.). Anhydrous rhyolite composition: Bishop Tuff sample BT87-2 [Wallace et al. 1999] using an  $Fe_2O_3/FeO$  ratio calculated at the quartz-fayalite-magnetite buffer using the model of Kress and Carmichael [1991].

ties from melt inclusions, which may lose significant  $\rm H_2O$  due to diffusive re-equilibration during storage in a region shallower than the original inclusion entrapment depth. At constant T, the effect of changing P on melt density is stronger in rhyolite than in basalt, due to the compressibility of  $\rm SiO_2$ . The effect is slightly more pronounced at higher  $\rm H_2O$  concentrations. At 1,000 °C and 10 wt%  $\rm H_2O$ , basalt densities range from 2.2—2.9 g/cm³ ( $d\rho/dP=2.4\times10^{-5}$  g/cm³-bar) while rhyolite densities range from 1.9–2.7 g/cm³ ( $d\rho/dP=2.8\times10^{-5}$  g/cm³-bar).

## 5 Applications to high-P melts

In the years since the development of the Lange and Carmichael [1990] equation of state and the publication of the partial molar properties used in DensityX (Table 1), significant progress has been made on the properties of melts, including density, over a wide range of compositions and H<sub>2</sub>O concentrations [San-

loup 2016; Terasaki and Nishida 2018]. Many of these recent works employed density measurements for various melts up to pressures well exceeding the limits of DensityX (≫100 kbar). It has been illustrated that third order Equations of State become necessary to accurately predict densities of melts at very high pressures due to changes in the coordination of various cations [Sanloup et al. 2013a; Sanloup et al. 2013b]. Figure 3 shows a comparison of density estimates by DensityX to those reported from recent in situ density measurements up to 30 kbar. DensityX reproduces the majority of reported densities to within a  $2\sigma$  error of 5% (indicated by dashed lines). Thus, the database used for DensityX remains valid up to at least 30 kbar in light of recent advancements regarding very high pressure melts.

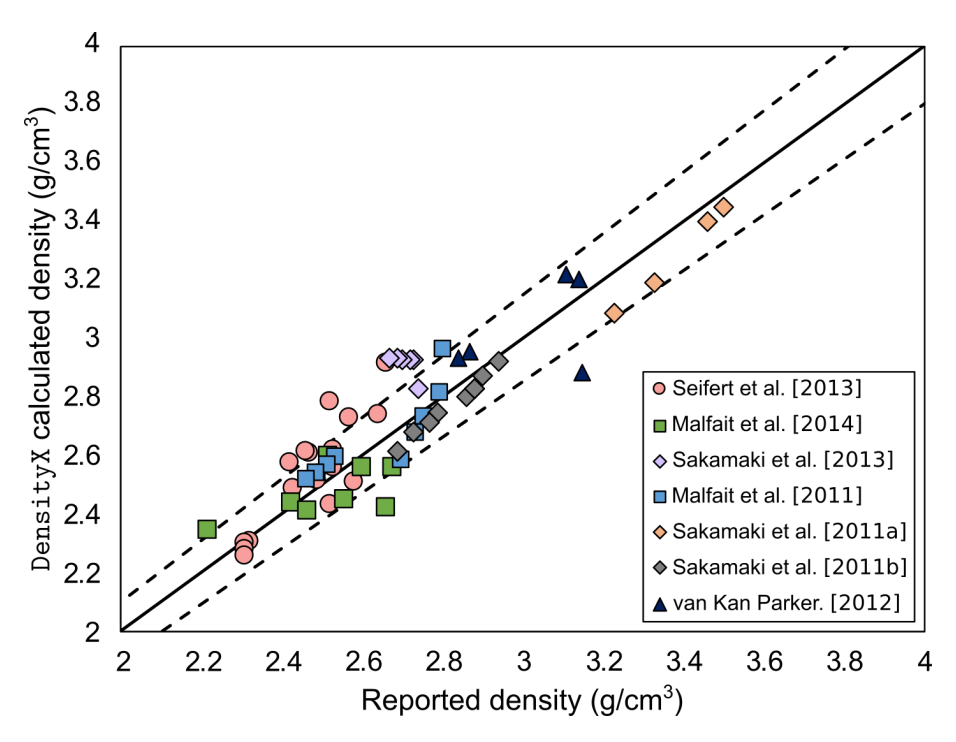


Figure 3: Comparison of silicate melt densities calculated with DensityX and measured in situ at high P and T. Black line is a 1:1 line. Dashed lines represent a  $2\sigma$  error envelope, equivalent to 5% relative. Reported densities are for: phonolitic melts [Seifert et al. 2013]; andesitic melts [Malfait et al. 2014]; basaltic melts [Sakamaki et al. 2013]; haplogranite, andesite, and basalt melts [Malfait et al. 2011]; high-Ti lunar basalts [Sakamaki et al. 2010a; van Kan Parker et al. 2012]; and peridotite melt [Sakamaki et al. 2010b].

## 6 Example application to density-driven convection in the Mount Erebus lava lake

Density-driven convection in volcanic systems is sometimes invoked to explain the growth of large, zoned crystals. This process is exemplified in systems with continuously convecting lava lakes, such as Erebus (Antarctica) and Nyiragongo (Democratic Republic of Congo), which host zoned megacrysts up to 10 cm At Erebus, oscillatory chemical zones in anorthoclase megacrysts erupted from the phonolite lava lake are thought to record magmatic convection cycles reaching as deep as ~7 km (2,000 bar) with little to no temperature change during convective cycling [Moussallam et al. 2015]. Evidence from crystal zones and observations of cyclicity in lava lake eruptive behavior (e.g. gas bubble bursts) and gas compositions provide good evidence that convection is driven by cycles of degassing at the surface followed by volatile replenishment in a shallow magma reservoir Oppenheimer et al. 2009; Ilanko et al. 2015].

Using DensityX, we calculated the pressure-density paths of volatile-bearing (0.2 wt%  $\rm H_2O$ ) and degassed Erebus phonolite lava between 0–2,500 bar at a constant T of 1000 °C (Figure 4). At magmatic temperatures, Erebus anorthoclase crystals have a density of 2.524 g/cm<sup>3</sup> [Moussallam et al. 2015], and as such remain negatively buoyant within anhydrous phono-

lite magma at pressures up to about 2,000 bar (illustrated in Figure 4). This is consistent with a scenario in which anorthoclase crystals continuously settle through a volatile-poor magma conduit [e.g. Molina et al. 2012] until they reach ~2,000 bar. The periodic infiltration of rehydrated magmas, which are positively buoyant relative to the surrounding degassed phonolite, could provide upward momentum sufficient to carry anorthoclase crystals back up toward the lava lake, recorded as cyclic chemical zoning in individual crystals. The exsolution of volatiles and generation of bubbles within upwelling magma will further decrease magma density, propelling it to the surface faster. Density curves in Figure 4 suggest that magma rehydration must occur at a minimum pressure of 2,000 bar, the point of neutral buoyancy for anorthoclase crystals within degassed phonolite melt. The actual rehydration pressure may be greater but would not be recorded by anorthoclase crystals, which are too buoyant to reach such depths.

DensityX does not consider the degassing of  $CO_2$ , which may have a significant effect on carbon-rich melts.  $CO_2$  has a larger partial molar volume than  $H_2O$  at the same temperature [Sakamaki et al. 2011] and so the addition of  $CO_2$  to the melt would decrease the density of volatile-bearing Erebus phonolite (Figure 4). However, despite Erebus's carbon-rich nature, lava lake phonolites are stored very shallowly and so are significantly degassed, containing only about 0.03 wt%  $CO_2$ 

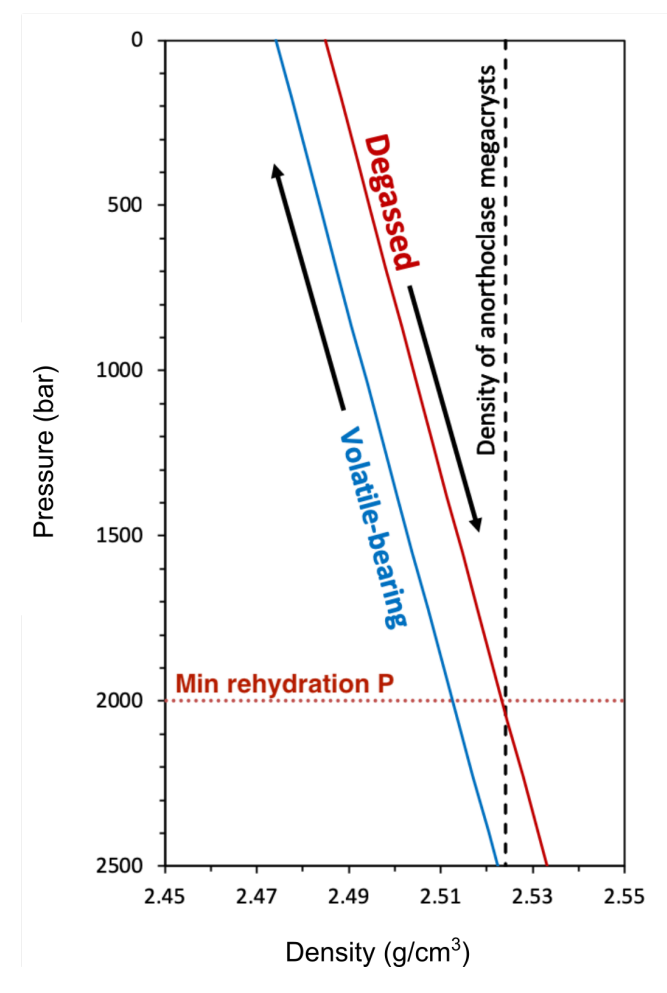


Figure 4: Density-driven convection within the shallow plumbing of Erebus volcano is likely the result of cycles of near-surface degassing followed by deep rehydration of phonolite melts at a minimum pressure of  $\sim 2,000$  bar (horizontal red dotted line). Low-density volatile-bearing melts (blue curve) rise to the surface where they degas and sink back into a shallow magma storage zone (red curve) where they are replenished with volatiles. This cycling is recorded in cyclic chemical zoning within anorthoclase megacrysts (black dashed line) that settle to a maximum depth of  $\sim 2,000$  bar and are carried upward during pulsatory ascent of hydrated magma batches.

[Iacovino 2015]. Thus, it is unlikely the addition of  $CO_2$  to our model would change our interpretations for Erebus drastically.

Other parameters can affect the efficiency of crystal settling and buoyancy in a magma. For example, the high viscosity of Erebus phonolite suggests that there will be a competition between the crystal settling time and the upwelling time. This may result in retrograde cycles, where sinking crystals are pushed upward before having the chance to completely settle to their point of neutral buoyancy. Such complex cyclicity is observed in zoning patterns of natural anorthoclase megacrysts [Moussallam et al. 2015]. High phonolite

viscosity may also result in crystals being dragged below their point of neutral buoyancy at 2,000 bars, but it is unlikely that crystals could sink much below this limit before buoyant forces overcome melt viscosity.

#### 7 Conclusions

DensityX is a powerful and extensible tool for calculating densities of silicate melts at pressures up to 30 kbar and temperatures up to 1,627 °C. The program is written to be easily incorporated into existing code written in Python via the densityx PyPi library. In addition, a standalone Python script capable of performing density calculations on 1000s of samples using a provided Microsoft Excel input file and a standalone Microsoft Excel spreadsheet capable of calculating the density of a single sample allows DensityX to be utilized by users of almost any computer skill level. We have demonstrated that DensityX reproduces a wide range of experimentally measured silicate melt densities to within a  $2\sigma$  error of 5%. DensityX was used to calculate the densitypressure relationships of dry and hydrated phonolite melt from Erebus volcano (Antarctica). A comparison with the known density of anorthoclase megacrysts, which record dehydration-rehydration cycles in the upper Erebus conduit, allowed us to constrain the rehydration depth to a minimum pressure of 2,000 bar.

#### ACKNOWLEDGEMENTS

The authors would like to thank Matthew Steele-MacInnis for his support of this project and thoughtful discourse related to its publication and David C. Rynearson for help in deploying the heroku web portal. They also thank Mark Ghiorso, Erik Duesterhoeft, Chrystele Sanloup, Charles LeLosq, and an anonymous reviewer for insightful comments on the manuscript and Magdalena Oryaëlle Chevrel for editorial support. K.I. was supported by National Science Foundation Frontiers in Earth System Dynamics (FESD) grant no. 1338810.

#### **AUTHOR CONTRIBUTIONS**

KI conceived of the project, wrote the DensityX code and online interface, and authored the manuscript. CBT assisted with the example applications to crustal magma density and in writing the manuscript.

#### DATA AVAILABILITY

The DensityX program demonstrated in this manuscript is open-source and MIT licensed. The full version of this code, which supports multiple sample input, is written in Python and is available in the github repository <a href="https://github.com/kaylai/DensityX">https://github.com/kaylai/DensityX</a>. Den-

sityX is also available as a Python library through PyPi and can be installed using pip. The code for the PyPi library is hosted at the DensityX github page. The same code is hosted on a heroku webserver at <a href="http://densityx.herokuapp.com/">http://densityx.herokuapp.com/</a>, which allows end-users to use the tool via an online interface in a web browser without the need to download and run the Python code. Documentation of the tool is also available on the heroku web portal. A simplified version of this program is written as a Microsoft Excel spreadsheet, which is provided with this manuscript as Supplementary Material (Supplementary file 1 and Supplementary file 2) and is also available for download via the heroku web portal.

## COPYRIGHT NOTICE

© The Author(s) 2019. This article is distributed under the terms of the Creative Commons Attribution 4.0 International License, which permits unrestricted use, distribution, and reproduction in any medium, provided you give appropriate credit to the original author(s) and the source, provide a link to the Creative Commons license, and indicate if changes were made.

#### REFERENCES

- Agee, C. B. and D. Walker (1988). "Mass balance and phase density constraints on early differentiation of chondritic mantle". *Earth and Planetary Science Letters* 90.2, pp. 144–156. DOI: 10.1016/0012-821x(88) 90097-0.
- Chaussard, E. and F. Amelung (2014). "Regional controls on magma ascent and storage in volcanic arcs". *Geochemistry, Geophysics, Geosystems* 15.4, pp. 1407–1418. doi: 10.1002/2013gc005216.
- Circone, S. and C. Agee (1996). "Compressibility of molten high-Ti mare glass: Evidence for crystalliquid density inversions in the lunar mantle". *Geochimica et Cosmochimica Acta* 60.14, pp. 2709–2720. DOI: 10.1016/0016-7037(96)00117-2.
- Connolly, J. (2005). "Computation of phase equilibria by linear programming: A tool for geodynamic modeling and its application to subduction zone decarbonation". *Earth and Planetary Science Letters* 236.1-2, pp. 524–541. DOI: 10.1016/j.eps1.2005.04.033.
- Dixon, J. E., E. M. Stolper, and J. R. Holloway (1995). "An Experimental Study of Water and Carbon Dioxide Solubilities in Mid-Ocean Ridge Basaltic Liquids. Part I: Calibration and Solubility Models". *Journal of Petrology*. DOI: 10.1093/oxfordjournals.petrology.a037267.
- Duesterhoeft, E. and C. de Capitani (2013). "THE-RIAK\_D: An add-on to implement equilibrium com-

- putations in geodynamic models". *Geochemistry, Geophysics, Geosystems* 14.11, pp. 4962–4967. DOI: 10.1002/ggge.20286.
- Fluegel, A. (2007). "Global Model for Calculating Room-Temperature Glass Density from the Composition". *Journal of the American Ceramic Society* 90.8, pp. 2622–2625. DOI: 10.1111/j.1551-2916.2007.01751.x.
- Ghiorso, M. S. (2004). "An equation of state for silicate melts. II. Calibration of volumetric properties at 105 Pa". *American Journal of Science* 304.8-9, pp. 679–751. DOI: 10.2475/ajs.304.8-9.679.
- Ghiorso, M. S. and R. O. Sack (1995). "Chemical mass transfer in magmatic processes IV. A revised and internally consistent thermodynamic model for the interpolation and extrapolation of liquid-solid equilibria in magmatic systems at elevated temperatures and pressures". Contributions to Mineralogy and Petrology 119.2-3, pp. 197–212. DOI: 10.1007/bf00307281.
- Grove, T. L. and M. B. Baker (1983). "Effects of melt density on magma mixing in calc-alkaline series lavas". *Nature* 305.5933, pp. 416–418. DOI: 10.1038/305416a0.
- Guo, X., R. A. Lange, and Y. Ai (2014). "Density and sound speed measurements on model basalt (An–Di–Hd) liquids at one bar: New constraints on the partial molar volume and compressibility of the FeO component". Earth and Planetary Science Letters 388, pp. 283–292. DOI: 10.1016/j.epsl.2013.12.005.
- Hack, A. C. and A. B. Thompson (2011). "Density and Viscosity of Hydrous Magmas and Related Fluids and their Role in Subduction Zone Processes". *Journal of Petrology* 52.7-8, pp. 1333–1362. DOI: 10.1093/petrology/egq048.
- Iacovino, K. (2015). "Linking subsurface to surface degassing at active volcanoes: A thermodynamic model with applications to Erebus volcano". *Earth and Planetary Science Letters* 431, pp. 59–74. DOI: 10.1016/j.eps1.2015.09.016.
- Ilanko, T., C. Oppenheimer, A. Burgisser, and P. Kyle (2015). "Transient degassing events at the lava lake of Erebus volcano, Antarctica: Chemistry and mechanisms". *GeoResJ* 7, pp. 43–58. doi: 10.1016/j.grj. 2015.05.001.
- Jull, M. and P. B. Kelemen (2001). "On the conditions for lower crustal convective instability". *Journal of Geophysical Research: Solid Earth* 106.B4, pp. 6423–6446. DOI: 10.1029/2000jb900357.
- Kress, V. C. and I. S. E. Carmichael (1991). "The compressibility of silicate liquids containing Fe2O3 and the effect of composition, temperature, oxygen fugacity and pressure on their redox states". *Contributions to Mineralogy and Petrology* 108.1-2, pp. 82–92. DOI: 10.1007/bf00307328.

- Lange, R. A. (1997). "A revised model for the density and thermal expansivity of K 2 O-Na 2 O-CaO-MgO-Al 2 O 3 -SiO 2 liquids from 700 to 1900 K: extension to crustal magmatic temperatures". *Contributions to Mineralogy and Petrology* 130.1, pp. 1–11. DOI: 10.1007/s004100050345.
- Lange, R. A. and I. S. Carmichael (1987). "Densities of Na2O-K2O-CaO-MgO-FeO-Fe2O3-Al2O3-TiO2-SiO2 liquids: New measurements and derived partial molar properties". *Geochimica et Cosmochimica Acta* 51.11, pp. 2931–2946. DOI: 10.1016/0016-7037(87)90368-1.
- Lange, R. and I. S. Carmichael (1990). "Thermodynamic properties of silicate liquids with emphasis on density, thermal expansion and compressibility". *Reviews in Mineralogy and Geochemistry* 24.1, pp. 25–64.
- Liu, Q. (2006). "The partial molar volume of Fe2O3 in alkali silicate melts: Evidence for an average Fe3 coordination number near five". *American Mineralogist* 91.2-3, pp. 385–393. DOI: 10.2138/am.2006.1902.
- Malfait, W. J., C. Sanchez-Valle, P. Ardia, E. Medard, and P. Lerch (2011). "Amorphous Materials: Properties, Structure, and Durability: Compositional dependent compressibility of dissolved water in silicate glasses". *American Mineralogist* 96.8-9, pp. 1402–1409. DOI: 10.2138/am.2011.3718.
- Malfait, W. J., R. Seifert, S. Petitgirard, M. Mezouar, and C. Sanchez-Valle (2014). "The density of andesitic melts and the compressibility of dissolved water in silicate melts at crustal and upper mantle conditions". *Earth and Planetary Science Letters* 393, pp. 31–38. DOI: 10.1016/j.eps1.2014.02.042.
- Molina, I., A. Burgisser, and C. Oppenheimer (2012). "Numerical simulations of convection in crystal-bearing magmas: A case study of the magmatic system at Erebus, Antarctica". *Journal of Geophysical Research: Solid Earth* 117.B7, n/a–n/a. DOI: 10.1029/2011jb008760.
- Moussallam, Y., C. Oppenheimer, B. Scaillet, I. Buisman, C. Kimball, N. Dunbar, A. Burgisser, C. I. Schipper, J. Andújar, and P. Kyle (2015). "Megacrystals track magma convection between reservoir and surface". *Earth and Planetary Science Letters* 413, pp. 1–12. doi: 10.1016/j.eps1.2014.12.022.
- Ochs III, F. A. and R. A. Lange (1999). "The Density of Hydrous Magmatic Liquids". Science 283.5406, pp. 1314–1317. DOI: 10.1126/science.283.5406. 1314.
- Ohtani, E. (1985). "The primodial terrestrial magma ocean and its implication for stratification of the mantle". *Physics of the Earth and Planetary Interiors* 38.1, pp. 70–80. DOI: 10.1016/0031-9201(85)90123-2.
- Oppenheimer, C., A. S. Lomakina, P. R. Kyle, N. G. Kingsbury, and M. Boichu (2009). "Pulsatory magma supply to a phonolite lava lake". *Earth and Planetary Science Letters* 284.3-4, pp. 392–398. DOI: 10.1016/j.eps1.2009.04.043.

- Richet, P., A. Whittington, F. Holtz, H. Behrens, S. Ohlhorst, and M. Wilke (2000). "Water and the density of silicate glasses". *Contributions to Mineralogy and Petrology* 138.4, pp. 337–347. DOI: 10.1007/s004100050567.
- Sakamaki, T., E. Ohtani, S. Urakawa, A. Suzuki, and Y. Katayama (2010b). "Density of dry peridotite magma at high pressure using an X-ray absorption method". *American Mineralogist* 95.1, pp. 144–147. DOI: 10. 2138/am.2010.3143.
- Sakamaki, T., E. Ohtani, S. Urakawa, H. Terasaki, and Y. Katayama (2011). "Density of carbonated peridotite magma at high pressure using an X-ray absorption method". *American Mineralogist* 96.4, pp. 553–557. DOI: 10.2138/am.2011.3577.
- Sakamaki, T., E. Ohtani, S. Urakawa, A. Suzuki, Y. Katayama, and D. Zhao (2010a). "Density of high-Ti basalt magma at high pressure and origin of heterogeneities in the lunar mantle". *Earth and Planetary Science Letters* 299.3-4, pp. 285–289. DOI: 10.1016/j.eps1.2010.09.007.
- Sakamaki, T., A. Suzuki, E. Ohtani, H. Terasaki, S. Urakawa, Y. Katayama, K.-i. Funakoshi, Y. Wang, J. W. Hernlund, and M. D. Ballmer (2013). "Ponded melt at the boundary between the lithosphere and asthenosphere". *Nature Geoscience* 6.12, pp. 1041–1044. DOI: 10.1038/ngeo1982.
- Sanloup, C., J. Drewitt, C. Crépisson, Y. Kono, C. Park, C. McCammon, L. Hennet, S. Brassamin, and A. Bytchkov (2013a). "Structure and density of molten fayalite at high pressure". *Geochimica et Cosmochimica Acta* 118, pp. 118–128. doi: 10.1016/j.gca.2013.05.012.
- Sanloup, C. (2016). "Density of magmas at depth". *Chemical Geology* 429, pp. 51–59. DOI: 10.1016/j.chemgeo.2016.03.002.
- Sanloup, C., J. W. E. Drewitt, Z. Konôpková, P. Dalladay-Simpson, D. M. Morton, N. Rai, W. van Westrenen, and W. Morgenroth (2013b). "Structural change in molten basalt at deep mantle conditions". *Nature* 503.7474, pp. 104–107. DOI: 10.1038/nature12668.
- Seifert, R., W. Malfait, S. Petitgirard, and C. Sanchez-Valle (2013). "Density of phonolitic magmas and time scales of crystal fractionation in magma chambers". *Earth and Planetary Science Letters* 381, pp. 12–20. doi: 10.1016/j.eps1.2013.08.039.
- Sparks, R. S. J. and H. E. Huppert (1984). "Density changes during the fractional crystallization of basaltic magmas: fluid dynamic implications". *Contributions to Mineralogy and Petrology* 85.3, pp. 300–309. DOI: 10.1007/bf00378108.
- Stolper, E., D. Walker, B. H. Hager, and J. F. Hays (1981). "Melt segregation from partially molten source regions: The importance of melt density and source region size". *Journal of Geophysical Research: Solid Earth* 86.B7, pp. 6261–6271. DOI: 10.1029/jb086ib07p06261.

DensityX IACOVINO & TILL, 2019

Terasaki, H. and K. Nishida (2018). "Density and Elasticity Measurements for Liquid Materials". *Magmas Under Pressure*. Elsevier, pp. 237–260. DOI: 10.1016/b978-0-12-811301-1.00009-5.

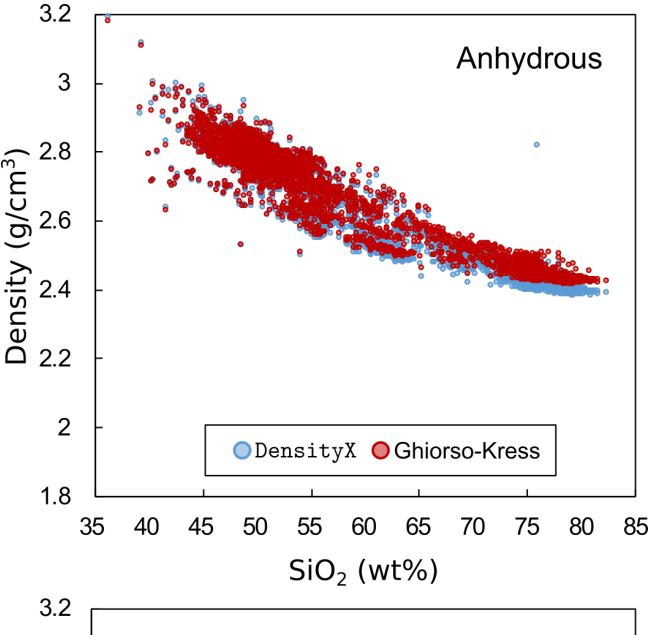
Van Kan Parker, M., C. Sanloup, N. Sator, B. Guillot, E. J. Tronche, J.-P. Perrillat, M. Mezouar, N. Rai, and W. van Westrenen (2012). "Neutral buoyancy of titanium-rich melts in the deep lunar interior". *Nature Geoscience* 5.3, pp. 186–189. DOI: 10.1038/ngeo1402.

Walker, G. P. L. (1989). "Gravitational (density) controls on volcanism, magma chambers and intrusions". Australian Journal of Earth Sciences 36.2, pp. 149–165. DOI: 10.1080/08120098908729479.

Wallace, P. J., A. T. Anderson, and A. M. Davis (1999). "Gradients in H2O, CO2, and exsolved gas in a large-volume silicic magma system: Interpreting the record preserved in melt inclusions from the Bishop Tuff". *Journal of Geophysical Research: Solid Earth* 104.B9, pp. 20097–20122. DOI: 10.1029/1999jb900207.

#### A APPENDIX 1

DensityX employs the equation of state (EOS) of Lange and Carmichael [1987]. The DensityX database (e.g. the experimental studies used to define partial molar volumes, thermal expansivities, and compressibilities) includes data used in Lange and Carmichael [1987], Kress and Carmichael [1991], and Lange [1997], and Ochs III and Lange [1999]. The resulting values used in the DensityX model are reported in Table 1. Since we do not employ the updated EOS of Ghiorso [2004], we likewise do not employ their expanded database. A comparison of densities calculated using DensityX with the DensityX database and the Ghiorso-Kress database (Figure A1) reveals that the two are generally in very good agreement, with an average discrepancy of <1% of the density value (maximum 3.04%).



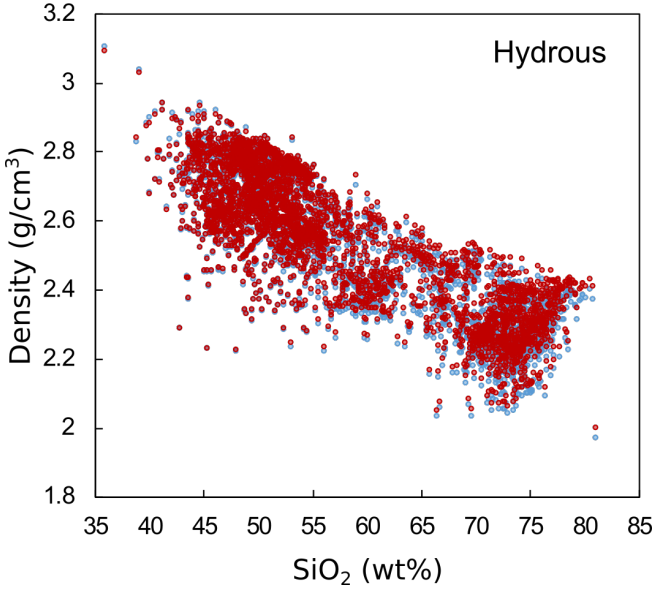


Figure A1: Comparison of densities of over 3,000 melt inclusions (normalized to 100%) from the GEOROC database calculated with DensityX (blue dots, same values as plotted in Figure 1) and with DensityX but using the Ghiorso-Kress expanded database (red dots). The average difference in values calculated with these two databases is <1% of the density value, with a maximum difference for any sample shown here of 3.04%.